# Delbrück scattering at energies of 140−450 MeV

Sh. Zh. Akhmadaliev, G. Ya. Kezerashvili, S. G. Klimenko, V. M. Malyshev, A. L. Maslennikov, A. M. Milov,
A. I. Milstein, N. Yu. Muchnoi, A. I. Naumenkov, V. S. Panin, S. V. Peleganchuk, V. G. Popov, G. E. Pospelov,
I. Ya. Protopopov, L. V. Romanov, A. G. Shamov, D. N. Shatilov, E. A. Simonov, and Yu. A. Tikhonov
*Budker Institute of Nuclear Physics, 630090 Novosibirsk, Russia*
(Received 29 June 1998)

The differential cross section of Delbrück scattering is measured on a bismuth germanate ($Bi_4Ge_3O_{12}$) target at photon energies 140–450 MeV and scattering angles 2.6–16.6 mrad. A good agreement with the theoretical results, obtained exactly in a Coulomb field, is found. [S0556-2813(98)02411-X]

PACS number(s): 13.60.Fz, 12.20.Fv, 25.20.Dc

## I. INTRODUCTION

Delbrück scattering [1] is a process in which the initial photon turns into a virtual electron-positron pair, is scattered in a Coulomb field of a nucleus, and then transforms into the final photon [Fig. 1(a)]. Thus, the final photon energy is equal to the energy of the initial photon (elastic scattering).

The interest in the experimental study of Delbrück scattering has the following motivations. First, it is one of the nonlinear quantum electrodynamic processes accessible at the present time to direct observation. Another such process is photon splitting in a Coulomb field [Fig. 1(b)]. For these processes the contribution of higher orders of the perturbation theory with respect to the parameter $Z\alpha$ ($Z|e|$ is the charge of the nucleus, $\alpha = e^2 = 1/137$ is the fine-structure constant, $e$ is the electron charge, $\hbar = c = 1$) at large $Z$ essentially modifies the cross section. Therefore, the investigation of these processes can be used as a good test of quantum electrodynamics in a strong electromagnetic field. Second, Delbrück scattering is the background process to the nuclear Compton scattering, which is an effective experimental tool to study mesonic and nucleon internal degrees of freedom of nucleus [2].

At present, four methods of Delbrück scattering amplitude calculation are used, possessing different areas of applicability:

(I) The amplitude is calculated in the lowest in $Z\alpha$ order of the perturbation theory, but for an arbitrary photon energy $\omega$ and scattering angle $\theta$. The review of numerous results, obtained in this approximation, can be found in [3,4]. These results are applicable only at small $Z$, when the parameter $Z\alpha \ll 1$.

(II) At high photon energies $\omega \gg m$ ($m$ is the electron mass) and small scattering angles $\theta \ll 1$ the amplitude is obtained by summing in a definite approximation of Feynman diagrams with an arbitrary number of photons exchanged with a Coulomb center [5].

(III) At $\omega \gg m$ and $\theta \ll 1$ it is possible to use also the quasiclassical approach [6], since in this case the momentum transfer $\Delta = |\mathbf{k}_2 - \mathbf{k}_1| = \omega\theta$ ($\mathbf{k}_1$ and $\mathbf{k}_2$ being the momenta of the initial and final photons, respectively), and the characteristic angular momentum $l \sim \omega/\Delta = 1/\theta \gg 1$. Numerically, approaches II and III lead to the same results, as they should, and show the significant difference between the cross section

calculated exactly in $Z\alpha$ and the cross section obtained in the lowest order of the perturbation theory.

(IV) At $\omega \gg m$ and $\theta \sim 1$ the amplitude is calculated exactly in $Z\alpha$ but neglecting the electron mass as compared to $\omega$ and $\Delta$ [7,8]. The approach is based on the use of the relativistic electron Green function in a Coulomb field. In this case the Coulomb effects are also significant.

The numerical results for the Delbrück scattering amplitudes obtained with the use of all four methods at different $\omega$, $\theta$, and $Z$ can be found in Ref. [9]. In our work we use the results obtained with method III, which is applicable under the conditions of our experiment.

In the experimental investigations of Delbrück scattering carried out earlier, three different photon sources have been used:

(1) Photons from the radioactive sources, for instance $^{24}$Mg ($\omega = 2.75$ MeV) [10,11].

(2) Photons from the nuclear-reactions-like capture of thermal neutrons in the energy range $\omega = 4-12$ MeV [12,13].

(3) In the energy range 20–100 MeV the experiment has been carried out with tagged bremsstrahlung photons [14]. In the experiment [15] Delbrück scattering above 1 GeV has been investigated using bremsstrahlung photons without tagging.

The accuracy of photon scattering cross-section measure-
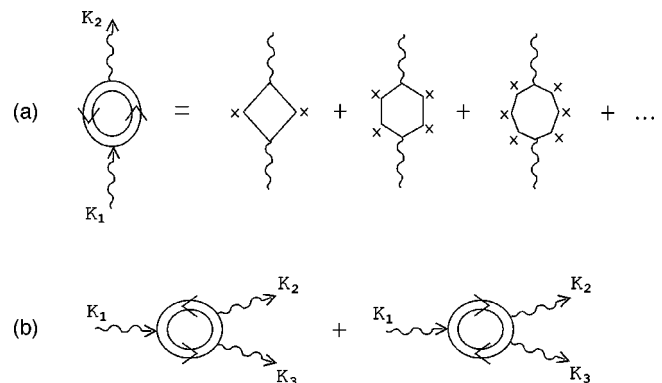


FIG. 1. (a) Feynman diagrams for Delbrück scattering: the Furry representation and the representation via the usual diagrams of the perturbation theory. The double line denotes the electron Green function in the Coulomb field, crosses denote the Coulomb field. (b) Feynman diagrams in the Furry representation for photon splitting.

FIG. 2. The experimental setup.

FIG. 3. The energy spectrum of the incoming tagged photons.
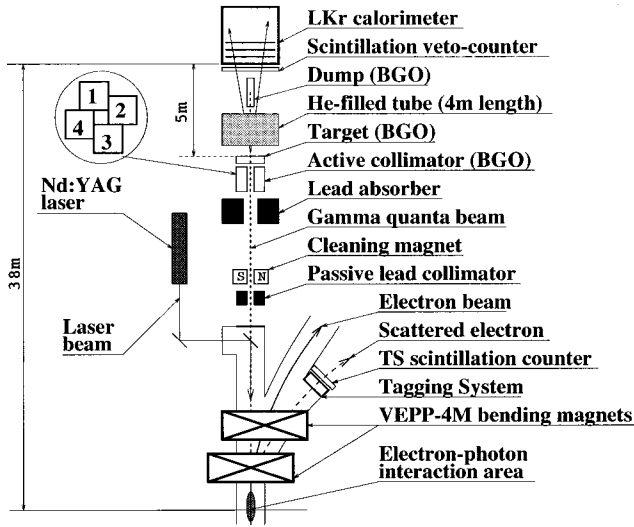
ments in the experiments [10–13] allowed one not only to observe Delbrück scattering, but to establish the importance of the Coulomb corrections to the cross section as well. Unfortunately, in this energy range ($\omega \sim m$) the Coulomb corrections have not been calculated up to now, which prevents us from performing the detailed comparison between experiment and theory.

At $\omega \gg m$ the amplitudes of Delbrück scattering are calculated including Coulomb corrections. However, the accuracy of the cross-section measurements achieved in the experiments [14,15] is essentially smaller than the accuracy of the theoretical predictions.

In the present experiment tagged backscattered Compton photons of energies 140–450 MeV were used. The final photons were detected at the scattering angles 2.6–16.6 mrad. At the specified parameters the theoretical predictions based on the quasiclassical approach (method III) have high accuracy, errors of the calculation are less than 1%. At the same time the experimental technique used has allowed us to get the high accuracy of the cross section measurements and, as a result, to make the detailed comparison between theory and experiment.

Apart from Delbrück scattering, we have investigated the process of photon splitting, which has been observed. Data analysis and comparison with the accurate theoretical predictions for this process are in progress now, the preliminary results can be found in [16]. Here we only note that the experimental data within the experimental accuracy ($\sim$10%) are in agreement with the results of recent theoretical calculations performed exactly in $Z\alpha$ [17].

## II. EXPERIMENTAL SETUP

The experiment has been carried out using ROKK-1M facility [18] of VEPP-4M collider [19]. The experimental setup is shown in Fig. 2. It includes the solid-state laser, an optical system of laser beam injection to the vacuum chamber of collider, and the photon tagging system [20] of the detector KEDR [21].

High-energy photons are produced as a result of laser photons backward Compton scattering on the electron beam.
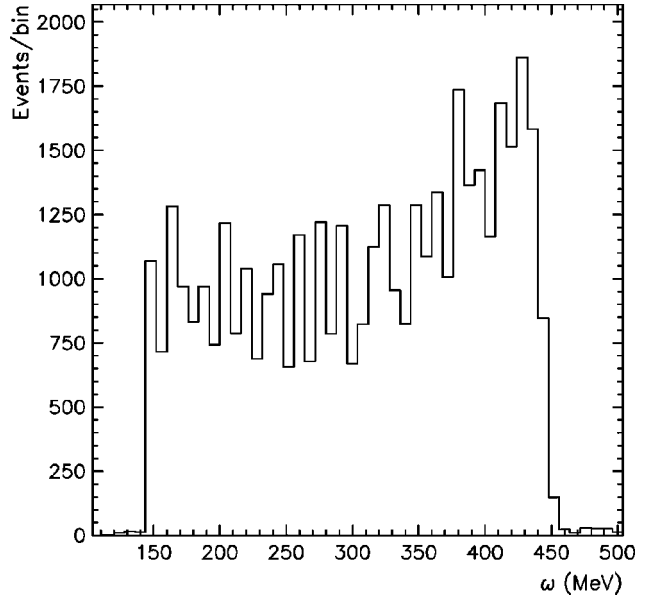
Scattered photons move along the electron beam and have a narrow angular spread of the order $1/\gamma$, where $\gamma$ is the electron relativistic factor. The photon energy spectrum has a sharp edge with the maximum energy, determined by the following expression:

$$E_{\max} = \frac{4\omega_L \gamma^2}{1 + 4\omega_L \gamma/mc^2},$$

where $\omega_L$ is the laser photon energy (1.17 eV). The energy of electron beam in experiment was 5.25 GeV, and $E_{\max}$ =451 MeV.

The scattered electron is removed from the beam by bending magnets of the accelerator and falls on the drift tubes hodoscope of the tagging system. The tagging system allows one to measure the energy of the scattered photon with the accuracy about 1.3%. The minimum energy of tagged photons in the experiment was 140 MeV.

The clean photon beam of the small transverse sizes is formed by the system of three collimators. The first lead
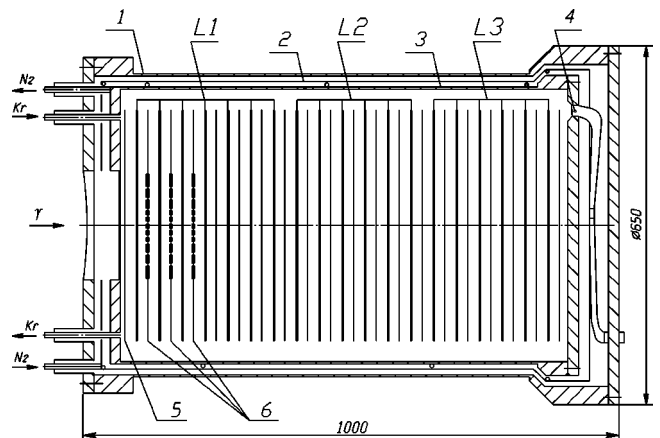
FIG. 4. The layout of the calorimeter: external vessel (1), copper shield (2), internal vessel (3), signal cable (4), veto electrode (5), strip electrodes (6), towers ($L1, L2, L3$).
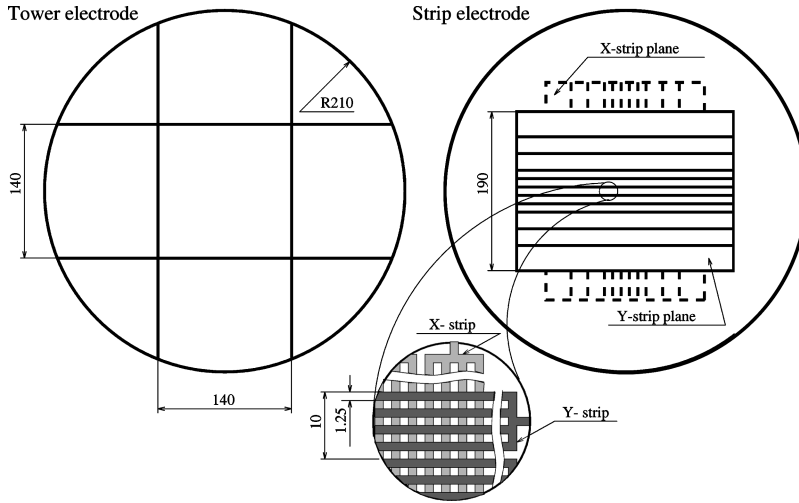
FIG. 5. The electrode structure of the calorimeter.

collimator has the 10 cm thickness, $4 \times 4$ mm$^2$ aperture, and it actually sets the transverse sizes of the beam. Charged particles of beam halo after this collimator are removed by the sweeping magnet with the magnetic field of 550 G. The second lead collimator, having the 30 cm thickness and 25 mm the diameter of the hole, is placed at 13 m from the first one. It absorbs secondary particles scattered on large angles. Behind this collimator the third active collimator is placed. It is formed by four BGO crystals of the transverse sizes of $25 \times 25$ mm$^2$ and 150 mm length. An aperture of this collimator ($9 \times 9$ mm$^2$) was chosen so that its inner edges could not see the interaction point of the laser photon beam and electron beam. Scintillation light from each BGO crystal of this collimator is detected by the photomultiplier. The signal of photomultipliers is included in the trigger of the experiment in anticoincidence. The active collimator removes the impurity of secondary particles moving in small angles with respect to the main photon beam.

The target is placed directly behind the last collimator. It is a BGO crystal of 12 mm thickness (1.07 radiation length)

and $25 \times 25$ mm$^2$ transverse sizes. Light from the crystal is detected by two photomultipliers, which signals are included in a trigger in anticoincidence. It enables us to suppress effectively a background from inelastic processes in the target at the trigger level. The threshold for the energy deposition in the target was set at the level of 150 KeV.

In order to reduce the background from Compton scattering after the target, photons pass the distance between the target and particle detector (4.8 m) in a helium-filled tube of 30 cm diameter. The photon-passed target without interaction falls onto an absorber installed before the aperture window of the detector. The absorber is a BGO crystal cylinder of 23 mm diameter and 146 mm length. Its signal is also included in a trigger in anticoincidence. It permits one to exclude the trigger start up from the photons, passed target without interaction. To suppress the trigger start up from the charged particles, a thin scintillation veto-counter is mounted on the aperture window of the detector.

The signals from the BGO collimator, target, absorber,
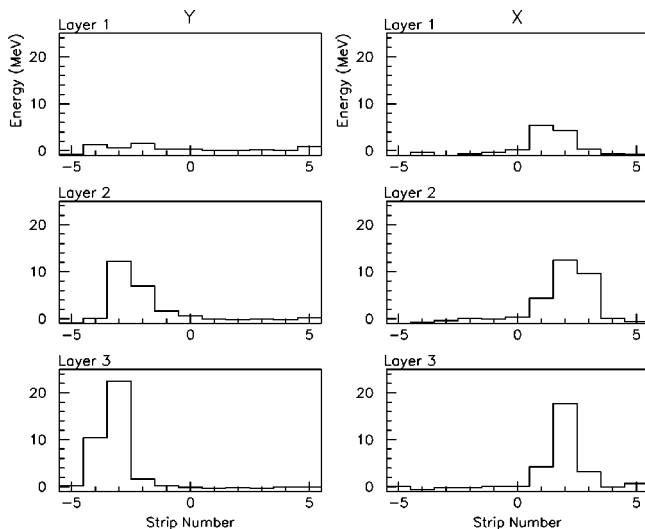


FIG. 6. The energy deposition on the strips for the event with the detected photon (the reconstructed coordinates are $X = 1.46$ cm, $Y = -2.56$ cm).
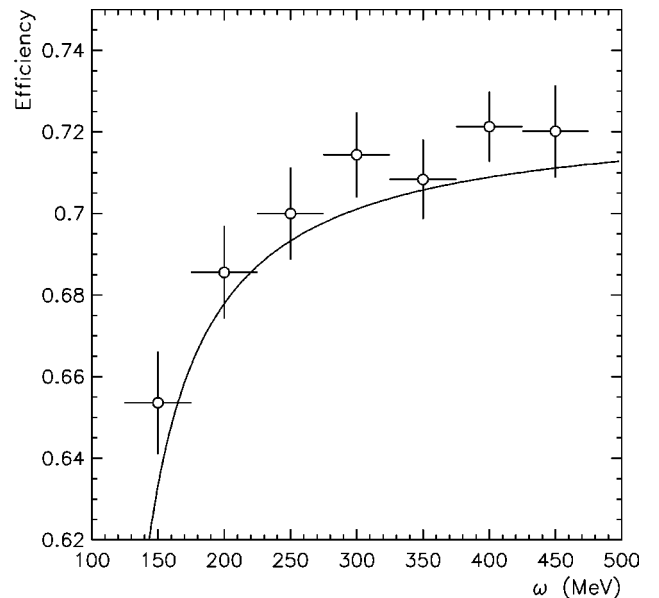


FIG. 7. The efficiency of the photon detection: experiment (circles), simulation (line).
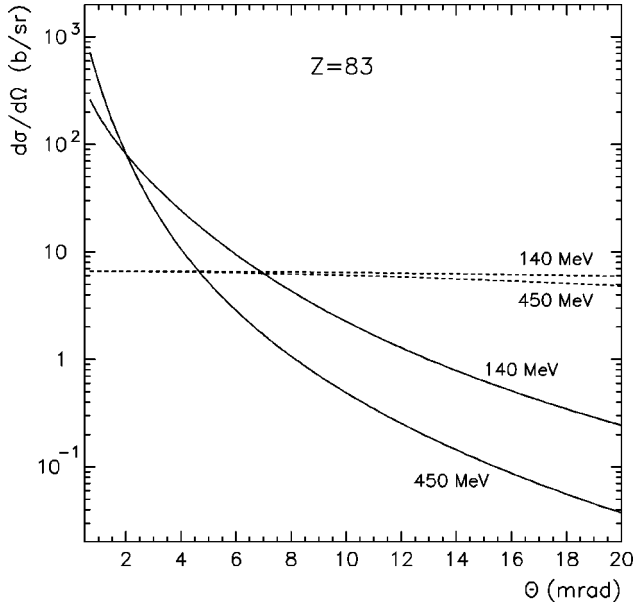
FIG. 8. The differential cross section for Delbrück (solid lines) and Compton (dashed lines) scattering on bismuth.

and veto counter are digitized and used in off-line analysis for the background suppression. Besides, the signals from the target and absorber are used to monitor the input $\gamma$ flux. The typical rate of the initial photons in the experiment was 5–10 kHz. These signals are exploited also to form an additional trigger to start the readout of the tagging system for measurement of the energy spectrum of initial photons (Fig. 3).

The final photons are detected by means of the electromagnetic calorimeter based on liquid krypton [22]. The layout of the calorimeter is shown in Fig. 4.

The electrodes are made of G10 sheets covered with a copper foil on both sides. The first (counting from the input window of the calorimeter) and all the odd electrodes are under zero potential (''grounded'' electrodes), high voltage is applied to all the even electrodes.

The high-voltage electrodes are used for energy measurements. They are divided into the 9 pads centered around the beam axis. In the longitudinal direction the electrode system is segmented into three sections, altogether the calorimeter contains 27 cells for energy measurements.

The ''grounded'' electrodes, from second to fourth, are used for the coordinate measurements. Strips are present on the both sides of these electrodes and oriented perpendicularly one to another. It enables us to measure both transverse coordinates ($X$ and $Y$) in one layer. The strip width varies from 1 cm in the center to 3 cm on the edge of the calorimeter's aperture. The structure of high-voltage and coordinate electrodes is shown in detail in Fig. 5. For such coordinate structure of the calorimeter, the space resolution is equal to 1 mm in the center and 2.3 mm on the edge.

The high-energy resolution of the calorimeter $[2.4\%/\sqrt{E(\text{GeV})}]$ and photon tagging allow to use effectively the equality of the initial and final photon energies in Delbrück scattering in order to suppress the background from inelastic processes.

On the initial step of the off-line analysis we select the events (named below as events with a detected photon) satisfying the following criteria:

(1) One track in the tagging system is found.

(2) Energy deposition in the crystals of the BGO collimator and in the absorber is less than 0.35 MeV.

(3) Energy deposition in the target is less than 0.15 MeV.

(4) Energy deposition in the scintillation counter on the aperture window of the calorimeter is less than 0.4 MeV.

(5) Energy deposition in the central tower of the first layer of the calorimeter is more than 80 MeV.

(6) One photon in the calorimeter is detected.

In Fig. 6 the example of the event with the detected photon is shown. In this event photon conversion has happened in the first $X$ layer.

The efficiency of the photon detection in the calorimeter is about 70% and weakly depends on the photon energy at $\omega > 140$ MeV (Fig. 7). The experimental data shown in Fig. 7 were obtained in runs when the target and absorber were removed. It is seen from this picture that the experimental efficiency is slightly higher than in the simulation. Therefore, in the comparison between the simulation and experiment this difference was taken into account.

## III. BACKGROUND PROCESSES FOR DELBRÜCK SCATTERING

The total cross section of Delbrück scattering at $\omega \gg m$ is independent of the photon energy, and the main contribution to it comes from scattering angles $\theta \sim m/\omega$. In the experiment the photons with the scattering angles 2.6–16.6 mrad were detected. For bismuth ($Z=83$) the cross section of Delbrück scattering in this range of angles is equal to 5.9 mb at
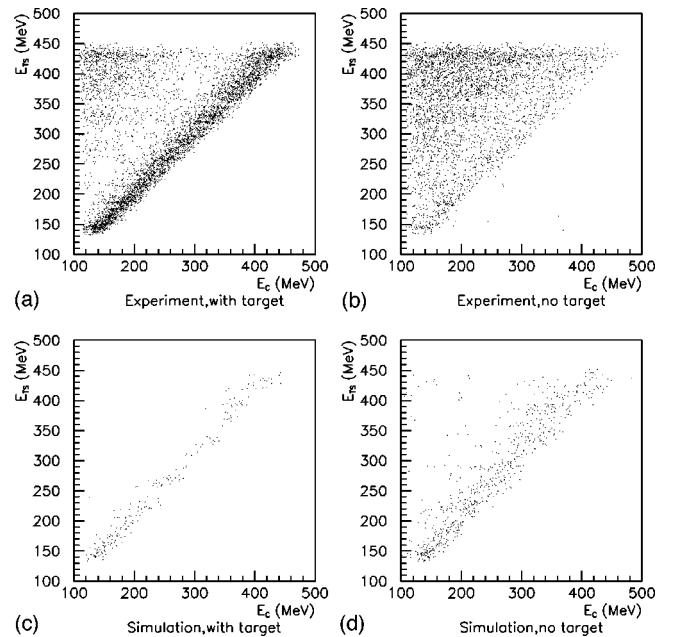


FIG. 9. The distributions of the energy deposition $E_C$ in the calorimeter versus the initial photon energy $E_{TS}$ for the events with the detected photons having scattering angles in the range 2.6–16.6 mrad. In simulation only processes included in GEANT are taken into account. Normalization corresponds to the number of the initial photons $1.5 \times 10^8$.
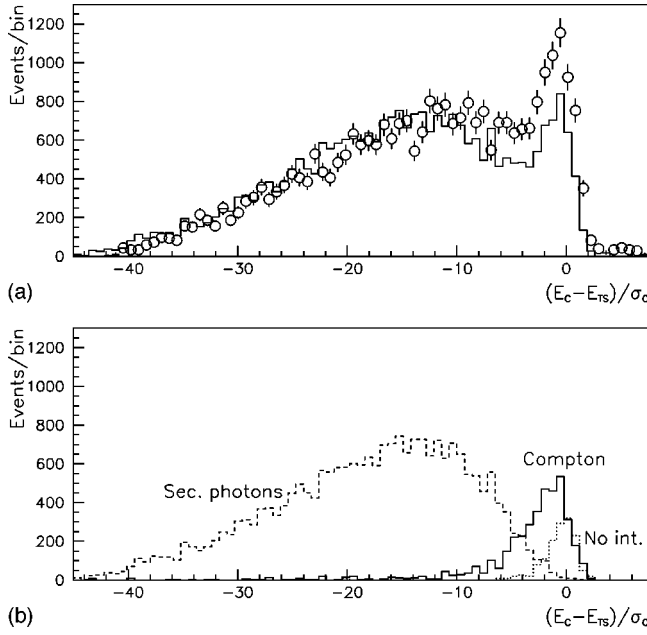
FIG. 10. The distributions of photons, detected in the range of angles 2.6–16.6 mrad for empty-target runs, over the parameter $(E_C - E_{TS})/\sigma_c$. (a) The experimental data (circles) and simulation (histogram, processes included in GEANT are only taken into account). (b) The contributions of different effects to the histogram (a): Compton scattering (solid line), secondary photons from showers (dashed line), photons passed the target and absorber without interaction (dotted line). The normalization corresponds to the number of the initial photons $10^9$.

$\omega = 140$ MeV and 1.2 mb at $\omega = 450$ MeV. For comparison, the total cross section for bismuth equals 6.4 mb. The contribution to the cross section from the scattering on germanium ($Z = 32$) for the range of angles under consideration is about 3%.
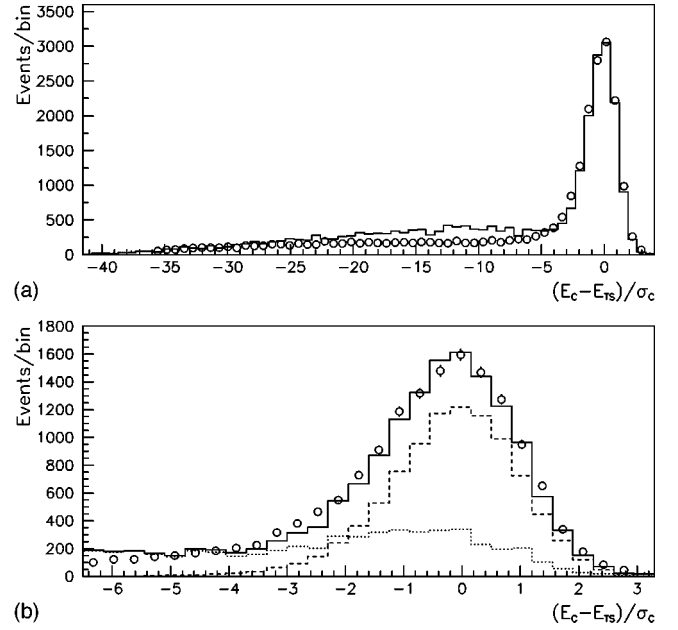


FIG. 11. The distributions of photons, detected in the range of angles 2.6–16.6 mrad for runs with the target, over the parameter $(E_C - E_{TS})/\sigma_c$. (a) The experimental data (circles) and simulation with the use of the GEANT package (histogram) including Delbrück scattering, photon splitting, and the background from the BGO collimator. (b) The experimental data (circles), simulation (solid line), Delbrück scattering (dashed line), and the sum of all background processes (dotted line). The normalization corresponds to the number of initial photons $10^9$.

Compton scattering on atomic electrons is the main background process under the conditions of our experiment. Its cross section for bismuth is about 5.3 and 4.9 mb at $\omega = 140$ and 450 MeV, respectively. The results of the calculations for differential cross sections of Delbrück and Compton scattering on bismuth are shown in Fig. 8.

TABLE I. The number of photons, detected in the range of angles 2.6–16.6 mrad at $\Delta E < 2.5\sigma_c$. The data in each column are normalized to the number of the initial photons $10^9$. The contributions of different processes are obtained in the simulation.

| $\omega$, MeV | 140–450 | 140–250 | 250–350 | 350–450 |
|---|---|---|---|---|
| Number of initial photons | $902.2 \times 10^6$ | $275.4 \times 10^6$ | $259.9 \times 10^6$ | $366.9 \times 10^6$ |
| Experiment | $13172 \pm 232$ | $16810 \pm 353$ | $13252 \pm 301$ | $10383 \pm 229$ |
| Simulation | $12810 \pm 181$ | $16709 \pm 329$ | $12535 \pm 283$ | $10079 \pm 209$ |
| Delbrück scattering | $9120 \pm 111$ | $12346 \pm 171$ | $8884 \pm 150$ | $6867 \pm 119$ |
| Compton scattering | $1334 \pm 45$ | $1624 \pm 85$ | $1254 \pm 80$ | $1173 \pm 66$ |
| Secondary photons | $52 \pm 8$ | $60 \pm 16$ | $57 \pm 16$ | $42 \pm 13$ |
| Photons passed without interaction | $495 \pm 62$ | $954 \pm 133$ | $324 \pm 65$ | $270 \pm 51$ |
| Photon splitting | $435 \pm 88$ | $434 \pm 90$ | $519 \pm 108$ | $376 \pm 78$ |
| Background from the BGO collimator | $1374 \pm 124$ | $1290 \pm 246$ | $1497 \pm 214$ | $1351 \pm 147$ |

TABLE II. The differential cross section of Delbrück scattering $d\sigma/dt$ for a molecule of bismuth germanate.

| $\Delta$ (MeV) | $\dfrac{d\sigma}{dt}$ (mb/MeV$^2$), calculation | $\dfrac{d\sigma}{dt}$ (mb/MeV$^2$), experiment |
|---|---|---|
| 0.49 | 21.1 | 19.9±3.4 |
| 0.62 | 12.9 | 10.1±1.2 |
| 0.75 | 8.30 | 8.10±0.62 |
| 0.88 | 5.55 | 5.25±0.36 |
| 1.01 | 3.83 | 3.88±0.25 |
| 1.14 | 2.72 | 3.07±0.18 |
| 1.27 | 1.99 | 2.09±0.13 |
| 1.40 | 1.49 | 1.66±0.11 |
| 1.53 | 1.13 | 1.12±0.08 |
| 1.66 | 0.883 | 0.966±0.073 |
| 1.79 | 0.696 | 0.758±0.064 |
| 1.92 | 0.555 | 0.569±0.059 |
| 2.05 | 0.450 | 0.476±0.056 |
| 2.18 | 0.369 | 0.410±0.055 |
| 2.31 | 0.306 | 0.356±0.045 |
| 2.44 | 0.255 | 0.238±0.049 |
| 2.57 | 0.215 | 0.148±0.038 |
| 2.70 | 0.183 | 0.139±0.035 |
| 2.83 | 0.157 | 0.187±0.035 |
| 2.96 | 0.135 | 0.151±0.028 |
| 3.09 | 0.116 | 0.112±0.030 |
| 3.22 | 0.101 | $(9.65\pm 2.7)\times 10^{-2}$ |
| 3.35 | $8.85\times 10^{-2}$ | 0.111±0.029 |
| 3.48 | $7.76\times 10^{-2}$ | $(9.0\pm 2.6)\times 10^{-2}$ |
| 3.61 | $6.83\times 10^{-2}$ | $(7.0\pm 2.3)\times 10^{-2}$ |
| 3.74 | $6.07\times 10^{-2}$ | $(6.7\pm 2.2)\times 10^{-2}$ |
| 3.87 | $5.37\times 10^{-2}$ | $(6.1\pm 2.1)\times 10^{-2}$ |

Secondary photons from showers, arising in target and air, give a very small contribution to the background. The low level of this background is the result of the following: the target in the experiment was "active," and the balance between the energy deposition in the calorimeter and the energy of the initial photon was required.

As simulation shows, there is also a small contribution to the background from photons passed the target and the absorber without interaction and, in consequence of the shower fluctuations in the calorimeter, detected at $\theta > 2.6$ mrad. The simulation was made with the use of the GEANT package (version 3.21).

Besides the Compton scattering and electromagnetic cascades (processes, included in GEANT), photon splitting was also taken into account as the background process. Since the cross section of this process is small in comparison with the cross section of the investigated effect, the approximate formula (the accuracy $\sim 20\%$) based on the Weizsäcker-Williams method was used for the calculation.

Other processes, such as Compton scattering on nuclei, $\pi^0$ photoproduction, and pair production with radiation of a photon, have been estimated under the conditions of the experiment. The first two processes give a negligible contribution to the number of scattered photons detected, while the contribution from the third one is about 0.5%.

Special attention was paid to the background, which comes from Compton and Delbrück scattering on the edges of the last BGO collimator. This question is discussed in Sec. IV.

## IV. EXPERIMENTAL RESULTS AND CONCLUSION

In order to understand the situation with the background, data has been taken in two modes: with the target and without the target ($9\times 10^8$ and $2\times 10^8$ photons, respectively).

In Figs. 9(a)–9(d) the two-dimensional distributions of energy deposition $E_C$ in the calorimeter versus the initial photon energy $E_{TS}$ for these modes are shown. The events with the detected photon having the scattering angle in the range 2.6–16.6 mrad are selected.

The diagonal band in Figs. 9(a) and 9(c) corresponds to the elastic scattering. In the simulation [Fig. 9(c)] this band contains the events of Compton scattering and the events, in which the initial photon passed the target and absorber without interaction and was detected in the given range of angles. The contribution to this band from showers in the target and air is very small. In the experimental distribution [Fig. 9(a)] this band is enhanced by virtue of Delbrück scattering in the target.

It is seen from Fig. 9 that in the experiment there is a large number of "inelastic scattering" events, i.e., the events with the energy deposition in the calorimeter essentially smaller than the energy of the initial photon. These events are the result of the electromagnetic showers generated in the BGO collimator by the initial photons touching it. Since this effect strongly depends on the position and orientation of the collimator with respect to the axis of the photon beam, it is not possible to simulate this effect accurately. Nevertheless, to subtract this background, one can use the experimental data of empty-target runs. In order to find the correct method of such subtraction, the simulation for empty-target runs was made. In the simulation the BGO collimator was shifted with respect to the axis of the initial photon beam so that 0.2% of
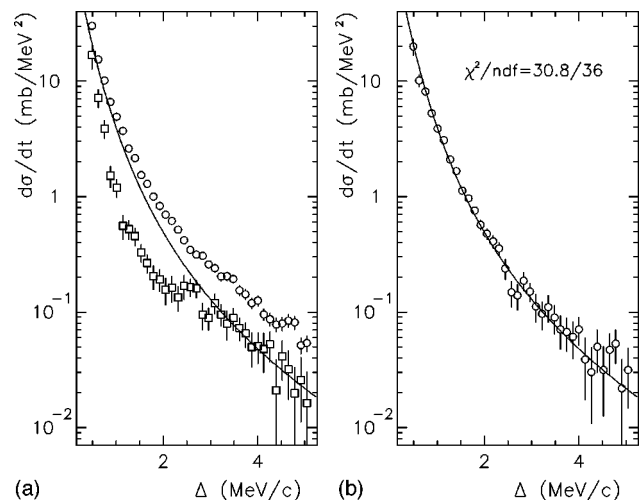


FIG. 12. The differential cross section of photon scattering $d\sigma/dt$ as a function of the momentum transfer $\Delta$ for a molecule of bismuth germanate. (a) The experimental data (circles) and the background (squares). (b) The experimental data after subtraction of the background (circles). The solid line is the result of the calculation.

photons touched it, and the signal from the collimator was not taken into account.

Figure 10 shows the distribution over the parameter $(E_C - E_{TS})/\sigma_c$ (where $\sigma_c$ is the energy resolution of the calorimeter) obtained as the result of such simulation. One can see that the contribution to the elastic scattering of secondary photons from showers (generated in the BGO collimator mainly), when $\Delta E = |E_C - E_{TS}| < 2.5\sigma_c$, is rather small. The small difference between simulation and experiment at $\Delta E < 2.5\sigma_c$ can be explained by the fact that Compton scattering in the BGO collimator cannot be simulated correctly, and Delbrück scattering in the collimator was not included in simulation in this case.

Thus, the background from the BGO collimator for runs with the target can be obtained as the difference between experiment and simulation for empty-target runs multiplied by the probability for photons to pass the target without interaction. This suppression factor is equal approximately to 0.5 and weakly depends on the energy at $\omega = 140-450$ MeV. This is correct at $\Delta E < 2.5\sigma_c$, while for events with $\Delta E > 2.5\sigma_c$, coming mainly from secondary photons, the suppression factor is bigger due to the charged component of the shower. It is illustrated by Fig. 11, which shows, for runs with the target, the distribution of scattered photons over the parameter $(E_C - E_{TS})/\sigma_c$ with taking this background into account.

In Table I we make the comparison between the experiment and the simulation for different energy ranges of the initial photon. The results of simulation for Delbrück scattering and the background processes are also shown. Errors in this table include the statistical errors as well as the total systematic error. The latter includes the error of measurement of the initial photons intensity and the error of photon detection efficiency (see Fig. 6). These errors are estimated to be 1.5% and 1%, respectively.

The differential cross section of Delbrück scattering for unpolarized photons is given by [4]

$$\frac{d\sigma}{d\Omega} = (Z\alpha)^4 r_0^2 \{|A^{++}|^2 + |A^{+-}|^2\},$$

where $r_0$ is the classical electron radius, $A^{++}$ and $A^{+-}$ are non-helicity-flip and helicity-flip amplitudes.

At $\omega \gg m$ and $\Delta \sim m$, as it was in the experiment, the helicity amplitudes have the form $A \sim \omega f(\Delta)$. Since $d\sigma/d\Omega$ is independent of azimuth angle $\varphi$, the differential cross section $d\sigma/dt$ is equal to $(\pi/\omega^2)d\sigma/d\Omega$ (where $t = \Delta^2$) and depends on the momentum transfer $\Delta$, but not on the photon energy $\omega$. It allows one to get the distribution $d\sigma/dt$ with the use of data for all energies of the initial photon (Table II and Fig. 12). It is seen from Table II and Fig. 12, that the experimental results are in good agreement with the theoretical predictions within the experimental accuracy.

[1] L. Meitner and H. Kösters, Z. Phys. **84**, 137 (1933).

[2] A. Baumann *et al.*, Nucl. Phys. **A536**, 87 (1992).

[3] P. Papatzacos and K. Mork, Phys. Rep. **21**, 81 (1975).

[4] A. I. Milstein and M. Schumacher, Phys. Rep. **243**, 184 (1994).

[5] M. Cheng and T. T. Wu, Phys. Rev. **182**, 1873 (1969); Phys. Rev. D **2**, 2444 (1970); **5**, 3077 (1972).

[6] A. I. Milstein and V. M. Strakhovenko, Phys. Lett. **95A**, 135 (1983); Sov. Phys. JETP **58**, 8 (1983).

[7] A. I. Milstein and R. Zh. Shaisultanov, J. Phys. A **21**, 2941 (1988).

[8] A. I. Milstein, P. Rullhusen, and M. Schumacher, Phys. Lett. B **247**, 481 (1990).

[9] H. Falkenberg *et al.*, At. Data Nucl. Data Tables **50**, 1 (1992).

[10] P. Rullhusen *et al.*, Z. Phys. A **293**, 287 (1979).

[11] B. Kasten *et al.*, Phys. Rev. C **33**, 1606 (1986).

[12] U. Zurmühl *et al.*, Phys. Lett. **114B**, 99 (1982).

[13] U. Zurmühl *et al.*, Z. Phys. A **314**, 171 (1983).

[14] A. Baumann *et al.*, Nucl. Phys. **A536**, 87 (1992).

[15] G. Jarlskog *et al.*, Phys. Rev. D **8**, 3813 (1973).

[16] Sh. Zh. Akhmadaliev *et al.*, *PHOTON'97, Incorporating the XIth International Workshop on Gamma-Gamma Collisions*, Egmond aan Zee, Netherlands, 246 (10-15/05/97).

[17] R. N. Lee, A. I. Milstein, and V. M. Strakhovenko, JETP **85**, 1049 (1997); Phys. Rev. A **57**, 2325 (1998).

[18] G. Ya. Kezerashvili *et al.*, in *High Energy Spin Physics*, edited by K. J. Heller *et al.*, AIP Conf. Proc. No. **343** (AIP, New York, 1995); p. 260.

[19] I. Ya. Protopopov, *Proceedings of XIII International Conference on High Energy Accelerators of Charged Particles*, Novosibirsk (1987), Vol. 1, p. 63.

[20] V. M. Aulchenko *et al.*, Nucl. Instrum. Methods Phys. Res. A **355**, 261 (1995).

[21] V. V. Anashin *et al.*, *Proceedings of International Symposium on Position Detectors in High Energy Physics*, 58, Dubna (1988).

[22] V. M. Aulchenko *et al.*, Nucl. Instrum. Methods Phys. Res. A **394**, 35 (1997).